AIAA JOURNAL
Vol. 46, No. 11, November 2008

Freestream Pulsation Effects on the Aeroelastic Response of a Finite Wing

Seung Ho Cho*
Samsung Thales Company, Ltd., Yongin 446-712, Republic of Korea
Taehyoun Kim†
The Boeing Company, Seattle, Washington 98124-2207
and
Seung Jin Song‡
Seoul National University, Seoul 151-742, Republic of Korea

DOI: 10.2514/1.33731

Existing aeroelastic analyses for finite wings have been mostly limited to cases with a steady freestream. In reality, however, the inflowing freestream can often be unsteady and pulsating. Therefore, this paper presents unsteady aerodynamic and aeroelastic analyses for a finite wing under a pulsating freestream. A new three-dimensional unsteady vortex lattice model under a pulsating freestream has been developed in discrete-time domain to examine unsteady aerodynamic forces acting on a vibrating wing. The structural behavior of the wing has been analyzed using a three-dimensional plate model. An aeroelastic model is then constructed by coupling the unsteady aerodynamic model with the structural model. Since the freestream velocity is assumed to be time-varying, the flutter onset of a wing under pulsating freestream is predicted by Floquet analysis. Numerical results of an untwisted and untapered wing show that the new time domain method can predict the aeroelastic stability as well as time history of the isolated wing under a pulsating freestream.

Nomenclature

AR	=	aspect ratio
D	=	stiffness matrix
E	=	coordinate transformation matrix
K	=	kernel function; stiffness matrix
L	=	total number of vortex elements in spanwise direction; generalized aerodynamic force
M	=	total number of bound vortex elements in chordwise direction; mass matrix
$M1$	=	total number of vortex elements on wing ($=M \times L$)
N	=	total number of bound and wake vortex elements in chordwise direction
$N1$	=	total number of vortex elements on wing and in wake ($=N \times L$)
n	=	time level; total number of mode shapes
q	=	velocity induced by vortex segment; generalized coordinates vector
U	=	freestream velocity
U_∞	=	mean freestream velocity
$\bar{u}$	=	magnitude of stream pulsations
w	=	downwash velocity
z	=	state vector
α	=	weighting factor
Γ	=	vortex strength
γ	=	mode shape
Δt	=	size of time step
Δx	=	size of vortex element in chordwise direction
Δy	=	size of vortex element in spanwise direction
ρ	=	structure density
ρ_∞	=	freestream air density
ϕ	=	chordwise mode shape
ψ	=	spanwise mode shape
Ω	=	frequency of stream pulsations

Subscripts

a	=	aerodynamic
s	=	structural
1	=	on wing; chordwise bending
2	=	in wake; spanwise bending
3	=	torsional

Received 30 July 2007; revision received 7 August 2008; accepted for publication 7 August 2008.

*Senior Engineer.
†Principal Engineer, Loads and Dynamics. Senior Member AIAA.
‡Professor, School of Mechanical and Aerospace Engineering.

I. Introduction

FLUID-STRUCTURE interactions occur in many scientific and engineering applications, and they include vibration and instability of aircraft wings and turbomachinery blades. Such fluid-structure interactions can cause structural fatigue and/or damage. Therefore, it is important to understand such phenomena, and aeroelastic analysis of aircraft wings involves coupling an unsteady aerodynamic model with a structural response model. Thus, flutter, which is a dynamic instability or self-excited vibration occurring at a certain flight speed (i.e., the flutter speed), can be predicted. To predict flutter onset and forced response of 2-D cascades and wings, unsteady incompressible aerodynamic models have been developed by Hall [1] and Kim et al. [2]. Though these approaches are time domain analyses, they can explicitly predict aeroelastic stability and are computationally less costly than unsteady computational fluid dynamics (CFD) methods. However, such analyses have been mostly limited to cases with a steady inflow.

The first attempt to derive a closed-form solution for pulsating freestream conditions was conducted by Isaacs [3]. At about the same time, Greenberg [4] extended Theodorsen's [5] theory to include pulsating freestream conditions. Later, Dugundji and Bundas [6] calculated unsteady aerodynamic forces on a rotating blade row under nonuniform inflow conditions to investigate the blade row's forced response. In this case, the flow nonuniformity in the absolute frame results in unsteady freestream conditions for rotating blades. Dugundji and Bundas assumed a small nonuniformity and did not

account for its influence on stability. Recently, Cho et al. [7] developed a time domain model to analyze the aeroelastic stability of an isolated two-dimensional wing under pulsating freestream conditions. In spite of such efforts, the effects of arbitrary magnitudes and frequencies of freestream pulsations on aerodynamics and flutter of an isolated *finite* wing still remain unknown.

Therefore, this paper presents aerodynamic and aeroelastic analyses for an isolated finite wing under a pulsating freestream. To address such issues, a new three-dimensional unsteady vortex lattice model under a pulsating freestream in discrete-time domain is presented. Then, the flutter onset of an isolated, untwisted, untapered, finite wing under a pulsating freestream is predicted via Floquet analysis. Finally, the forced response of an isolated rotating finite wing under a pulsating freestream is examined.

II. Model Description

A. Unsteady Aerodynamic Model

Unsteady aerodynamic forces on a single wing have been calculated using a three-dimensional unsteady vortex lattice method (Fig. 1). Because the aerodynamic quantity of interest in this study is lift, viscous effects are expected to be less important. The bound and free vortices, representing the wing and the traveling wake vortices, respectively, are modeled as vortex ring elements. There are M elements in the streamwise x direction, and L elements in the spanwise y direction on the wing. There are (N-M) elements in the streamwise direction in the wake. Thus, the total number of vortex ring elements is $M1$ ($=M \times L$) on the wing and $N1$ ($=N \times L$) for the combined wing and free wake. The wing elements are all of equal size. The element at the i, jth locations in the x and y coordinates is assigned a vortex strength Γ_{ij}. For convenience, a $(L \times 1)$ vector ${}^{i}\Gamma$ is defined as

$$ {}^{i}\Gamma = [\,\Gamma_{i1} \quad \Gamma_{i2} \quad \cdots \quad \Gamma_{iL}\,]^T \qquad (L \times 1) \tag{1} $$

With this definition, a downwash vector can be expressed in the discrete-time domain as

$$ w^n = [\,K_1^n \quad K_2^n\,] \begin{Bmatrix} \Gamma_1^n \\ \Gamma_2^n \end{Bmatrix} \qquad (M1 \times 1) \tag{2} $$

where w_i^n is a $(M1 \times 1)$ vector at time n. The two vectors Γ_1 $(M1 \times 1)$ and Γ_2 $[(N1 - M1) \times 1]$ are defined as

$$ \Gamma_1 = [\,{}^{1}\Gamma \quad {}^{2}\Gamma \quad \cdots \quad {}^{M}\Gamma\,]^T \qquad (M1 \times 1) \tag{3} $$

$$ \Gamma_2 = [\,{}^{M+1}\Gamma \quad {}^{M+2}\Gamma \quad \cdots \quad {}^{N}\Gamma\,]^T \qquad [(N1 - M1) \times 1] \tag{4} $$

where Γ_1 and Γ_2 represent arrays of vortex strengths for the wing and wake, respectively. For a vortex ring element in a three-dimensional incompressible flow, the kernel function K_{ij} of a unit vortex strength at the jth vortex point influences the velocity at the ith collocation point. The collocation points are at the three-quarter chord point in the streamwise direction and the central point in the spanwise direction of the bound vortex elements. The vortex points are at the quarter-chord point in the streamwise direction and the central point in the spanwise direction of the bound and free vortex elements [8]. Given a vortex strength Γ, the velocity induced by a vortex segment lm is

$$ q_{lm}(x, y, z) = \frac{\Gamma}{4\pi} \frac{\mathbf{r}_l \times \mathbf{r}_m}{|\mathbf{r}_l \times \mathbf{r}_m|^2} \left[\mathbf{r}_0 \cdot \left(\frac{\mathbf{r}_l}{r_l} - \frac{\mathbf{r}_m}{r_m} \right) \right] \tag{5} $$

In a pulsating freestream, the locations of the bound vortex segments r_l and r_m remain time invariant because the vortex segments can be assumed to be of equal size Δx on the wing. However, the locations of the wake vortices are time varying because the elemental length in the streamwise direction changes according to $\Delta x(t) = U(t)\Delta t$. Thus, the location of a wake vortex is

$$ r_j(t) = \int_{(n+M-j)\Delta t}^{n\Delta t} U(t)\, \mathrm{d}t \qquad (j = M+1, \ldots, N) \tag{6} $$

where the freestream velocity $U(t)$ is arbitrarily time varying. For this investigation, the freestream velocity is assumed to be time periodic. More specifically, for simplicity, it is assumed to be sinusoidal:

$$ U(t) = U_\infty + \bar{u} \cos \Omega t \tag{7} $$

The total velocity induced by a vortex ring element is the sum of q_{lm} for all four segments as follows:

$$ q^{\mathrm{tot}} = q_{12} + q_{23} + q_{34} + q_{41} = q_i^{\mathrm{tot}} \hat{i} + q_j^{\mathrm{tot}} \hat{j} + q_k^{\mathrm{tot}} \hat{k} \tag{8} $$

Ignoring the in-plane motion of the wing, the kernel function K_{ij} that governs the fluid-structure interaction is the vertical component of q_k^{tot} per unit vortex strength as follows:

$$ K_{ij} = q_k^{\mathrm{tot}} / \Gamma \tag{9} $$

The conservation of vorticity requires that

$$ {}^{M+1}\Gamma^{n+1} = {}^{M}\Gamma^{n} \tag{10} $$

and the convection of free wakes is described in discrete-time domain as follows:

$$ {}^{i}\Gamma^{n+1} = {}^{i-1}\Gamma^{n} \qquad (i = M+2, \ldots, N-1) \tag{11} $$

$$ {}^{N}\Gamma^{n+1} = \alpha^{N}\Gamma^{n} + {}^{N-1}\Gamma^{n} \qquad (0.95 < \alpha < 1) \tag{12} $$

With the weighting factor α in Eq. (12), one can cut off the infinitely long wake vortex at a finite length. For an isolated wing under steady flow, Hall has suggested $0.95 < \alpha < 1$ [1].

Combining the equations for the downwash [Eq. (2)], conservation of vorticity [Eq. (10)], and free wake convection [Eqs. (11) and (12)] leads to

$$ \Gamma_2^{n+1} = A\Gamma_1^n + B\Gamma_2^n \tag{13} $$

The bound vortex is eliminated via a static condensation as follows [9]:

$$ \Gamma_2^{n+1} = \{B - A(K_1^n)^{-1}K_2^n\}\Gamma_2^n + A(K_1^n)^{-1}w^n = A_a\Gamma_2^n + B_a w^n \tag{14} $$

B. Aeroelastic Model

Forces and moments acting on a three-dimensional plate are derived. Substituting the strain energy, kinetic energy, and work of the wing into the Lagrange's equation leads to the equation of motion as follows:

$$ M\ddot{q} + Kq = L \tag{15} $$

where K and M are the generalized mass and stiffness matrices, respectively. They are defined as

$$ M_{ij} = \iint_A \rho \gamma_i \gamma_j \, \mathrm{d}x \, \mathrm{d}y \tag{16} $$

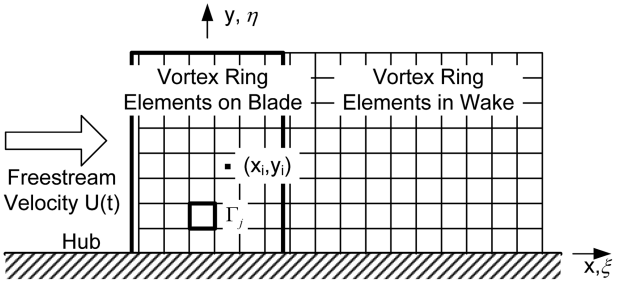

Fig. 1 Vortex ring elements for a single three-dimensional wing [1].

$$K_{ij} = \iint_A \left(D_{22} \frac{\partial^2 \gamma_i}{\partial y^2} \frac{\partial^2 \gamma_j}{\partial y^2} + 4D_{33} \frac{\partial^2 \gamma_i}{\partial x \partial y} \frac{\partial^2 \gamma_j}{\partial x \partial y} \right) \mathrm{d}x\, \mathrm{d}y \tag{17}$$

where D_{22} and D_{33} represent spanwise bending and torsional stiffness, respectively [9].

The structural equation of motion can be put in state-space form as follows:

$$\begin{Bmatrix} \dot{q} \\ \ddot{q} \end{Bmatrix} = \begin{bmatrix} O & I \\ -M^{-1}K & O \end{bmatrix} \begin{Bmatrix} q \\ \dot{q} \end{Bmatrix} + \begin{bmatrix} O \\ M^{-1} \end{bmatrix} L \tag{18}$$

Discretizing Eq. (18) in time, a discrete-time domain form is obtained as follows:

$$z^{n+1} = A_s z^n + B_a L^n \tag{19}$$

where z is a state vector $[\, q \quad \dot{q} \,]^T$.

The generalized aerodynamic force component for the ith mode shape can be approximated as

$$L_i \cong \sum_{l=1}^{L} \sum_{m=1}^{M} \Delta p_{ml} \phi_i(x_m) \psi_i(y_l) \Delta x \Delta y \qquad (i = 1, 2, \ldots, n) \tag{20}$$

where the subscripts m and l stand for the location of the (m, l)th vortex of strength Γ_{ml}. Using the unsteady Bernoulli equation, the pressure differential can be expressed as [8]

$$\Delta p_{ml} = \Delta p(x_m, y_l, t) = \rho_\infty \left\{ U(t) \left(\frac{\Gamma_{ml} - \Gamma_{m-1l}}{\Delta x} \right) + \dot{\Gamma}_{ml} \right\} \tag{21}$$

where the freestream velocity $U(t)$ is time varying. Using a forward difference formula, $\dot{\Gamma}_{ml}$ can be written in discrete-time domain as follows:

$$\dot{\Gamma}_{ml} \cong \frac{\Gamma_{ml}^{n+1} - \Gamma_{ml}^{n}}{\Delta t} \tag{22}$$

Equation (22) is then substituted into Eq. (21) to give

$$L_i^n = U(n\Delta t) V_1 \Gamma_i^n + U_\infty V_2 (\Gamma_i^{n+1} - \Gamma_i^n) \tag{23}$$

For a wing undergoing out-of-plane motion $w(x, y, t)$ and negligible in-plane motion $u(x, y, t)$, $v(x, y, t)$, the downwash vector is related to the generalized coordinates as

$$w = U(t) E_1 q + E_2 \dot{q} \tag{24}$$

The aeroelastic system consists of the unsteady aerodynamic model [Eq. (14)] and the structural model [Eq. (19)]. The generalized aerodynamic force [Eq. (23)] and the downwash vector [Eq. (24)] are also needed to couple the aerodynamic and structural models. The resulting system of $(N1 - M1 + 2n)$ equations is as follows:

$$\begin{bmatrix} I & O \\ O & I - B_s[\, B_3 \quad B_4 \,] \end{bmatrix} \begin{Bmatrix} \Gamma_2 \\ z \end{Bmatrix}^{n+1} = \begin{bmatrix} A_a & B_a[\, U(t)E_1 \quad E_2 \,] \\ B_s A_1 & A_s + B_s[\, B_1 \quad B_2 \,] \end{bmatrix} \begin{Bmatrix} \Gamma_2 \\ z \end{Bmatrix}^{n} \tag{25}$$

The preceding system is a periodic function of time. Therefore, its stability cannot be directly determined by standard eigenvalue analysis [1], and Floquet analysis is needed [10].

The Floquet method checks eigenvalues of the linear periodic system based on the monodromy matrix, which is obtained by integrating the system equations over one period subject to an initial condition matrix I. If real parts of all of the eigenvalues are less than zero, the system is asymptotically stable. The analysis, however, does not yield information on the frequency content of the system response. Also, its application to a large-scaled CFD model becomes impractical due to heavy computation associated with the time integration and the large size of the state transition matrix.

III. Model Predictions

A. Unsteady Aerodynamic Results

First, the new three-dimensional unsteady vortex lattice model is validated for a flat plate under a steady freestream. As in Hall [1], a flat plate with an aspect ratio of 5.0 has been assumed, and other relevant aerodynamic parameters are listed in Table 1. Figure 2 shows the nondimensional indicial lift

$$\frac{1}{2\pi} \frac{L}{1/2 \rho U_\infty^2 c L}$$

plotted versus the nondimensional time $\tau = U_\infty t / b$. The indicial lift is generated by a sudden rigid-body plunging motion of the plate (at $\tau = 0$). For the current steady flow case, the magnitude of freestream pulsations $\bar{u}$ has been set to zero in Eq. (7). The new three-dimensional vortex lattice method's prediction closely matches Hall's result [1].

Figure 3 shows the indicial lift under a steady flow for three-dimensional plates for various aspect ratios. For comparison, Fig. 3 also shows the Wagner's function, which is the two-dimensional analytical solution for flat plates [11]. The shapes of the lift time history curves are similar among all cases. As the aspect ratio of plate increases, the lift magnitude approaches the two-dimensional analytical solution. The slope and final value are also reduced with decreasing finite aspect ratio due to the effects of the tip relief, or the unloading at the wing tip. The tip unloading occurs due to pressure equalization between the bottom and top of the plate, and hence no lift is created at these points [12]. This trend can be seen more clearly in Fig. 4. In the figure, the nondimensional vortex strength Γ/Γ_0 is plotted versus the distance along the span $2y/l$ for various aspect ratios. Here, Γ_0 is the vortex strength at the midspan. The vortex strength is high at the plate midspan but rapidly drops to zero at the tip. The vortex strength distribution decreases as the aspect ratio is reduced. This result matches Prandtl's lifting-line theory. Thus, the results in Fig. 4 help explain the trend in Fig. 3 of the indicial lift's dependence on the aspect ratio.

The number of vortex elements required in both the chordwise and spanwise directions have been determined as follows. Figure 5 illustrates the indicial lift under a pulsating freestream plotted versus time for 24, 48, and 72 (bound and wake) vortex elements in the chordwise direction. In all three cases, the number of the wake vortex elements is 5 times that of the bound vortex elements. The freestream is assumed to be sinusoidal, and the nondimensional freestream fluctuation $\bar{u}/U_\infty$ has been set to 0.4. This value is equivalent to that used by Isaacs [3]. The pulsating freestream results are not sensitive to the number of elements in the chordwise direction for element numbers greater than 24. Hence, for the following results, the numbers of bound and wake vortex elements in the chordwise direction have been set to be 8 and 40, respectively (Table 1). Figure 6 is an analogous figure for 5, 10, and 15 vortex elements in the spanwise direction for $\bar{u}/U_\infty = 0.4$. For this freestream case, 10 vortex elements in the spanwise direction are sufficient.

Figure 7 illustrates the influence of the wing aspect ratio on the time history of the indicial lift under a pulsating freestream. Again, the magnitude of the sinusoidal freestream pulsations $\bar{u}/U_\infty$ has been set to 0.4. For nondimensional time τ less than about 10, the transient effects are visible, and such transients can be captured only through a time domain analysis. If the magnitude of freestream pulsations $\bar{u}$ is set to zero, the results in Fig. 3 are recovered. As the aspect ratio decreases, the magnitude of lift pulsation becomes smaller due to the tip unloading and weakening of the bound vortices.

Table 1 Aerodynamic input parameters of three-dimensional plate [1]

Parameters	Values
Aspect ratio	5
Bound vortex elements in chordwise direction	8
Wake vortex elements in chordwise direction	40
Vortex elements in spanwise direction	10
Weighting factor	0.992

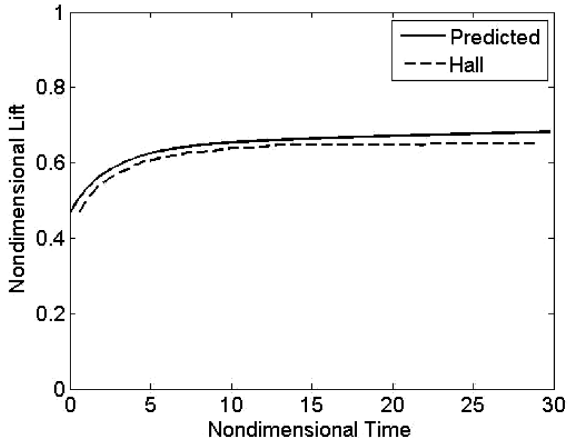

Fig. 2 Indicial lift under a steady freestream predicted by the new model and Hall's model [1].

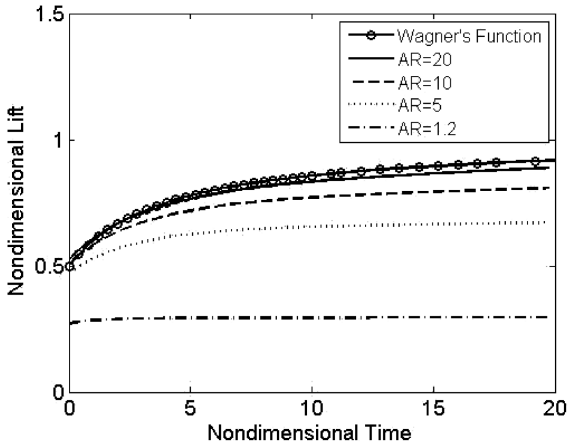

Fig. 3 Indicial lift under a steady freestream for various aspect ratios.

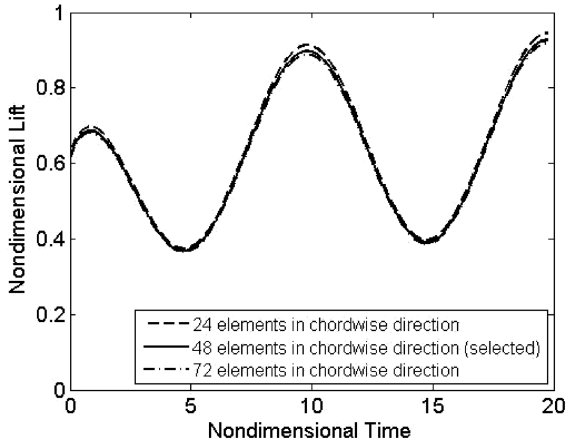

Fig. 5 Indicial lift under a pulsating freestream for various vortex elements in the chordwise direction when $\bar{u}/U_\infty = 0.4$.

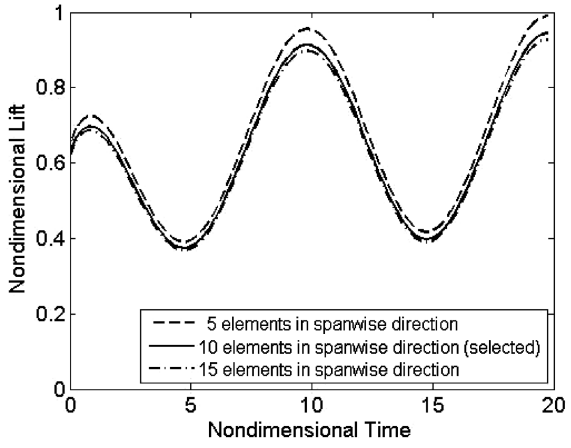

Fig. 6 Indicial lift under a pulsating freestream for various vortex elements in the spanwise direction when $\bar{u}/U_\infty = 0.4$.

The weakened bound vortices are then convected into the wake at the pulsating freestream speed and, thus, the indicial lift pulsation is decreased. However, the phase of the lift pulsations remains the same.

Figure 8 shows the indicial lift under a pulsating freestream for pulsation magnitudes $\bar{u}/U_\infty$ between 0.0 and 0.8. The magnitude of freestream pulsations is important for determining lift deviation and fatigue loading. The aspect ratio AR has been set to 5 because this value is commonly used for airplane wings [1]. When $\bar{u}/U_\infty = 0.0$, the indicial lift under steady freestream for $AR = 5$ (Fig. 2) is recovered. As $\bar{u}/U_\infty$ increases, the magnitude of lift pulsations also increases due to the combined effects of the increased variation in the wake vortex's location [Eq. (6)], and the deviation of the bound vortex strength [Eq. (2)].

B. Aeroelastic Stability Results

This section presents the aeroelastic results from the new three-dimensional unsteady vortex lattice model coupled with an existing structural model. In the current study, a plate model with the first four

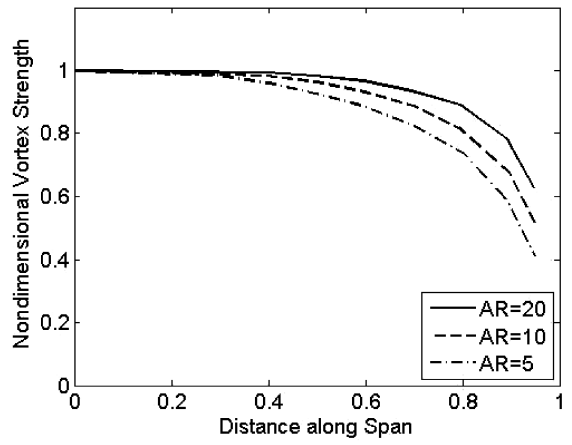

Fig. 4 Nondimensional vortex strength distributions for various aspect ratios.

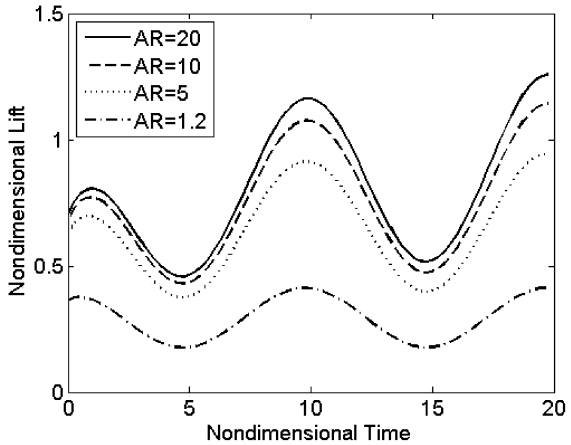

Fig. 7 Indicial lift under a pulsating freestream for various aspect ratios when $\bar{u}/U_\infty = 0.4$.

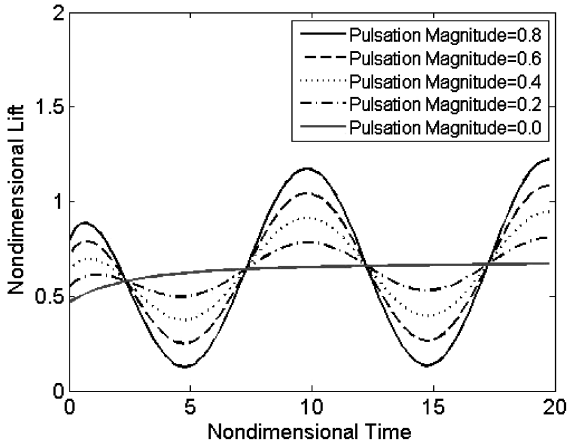

Fig. 8 Indicial lift under a pulsating freestream for various pulsation magnitudes when AR = 5.

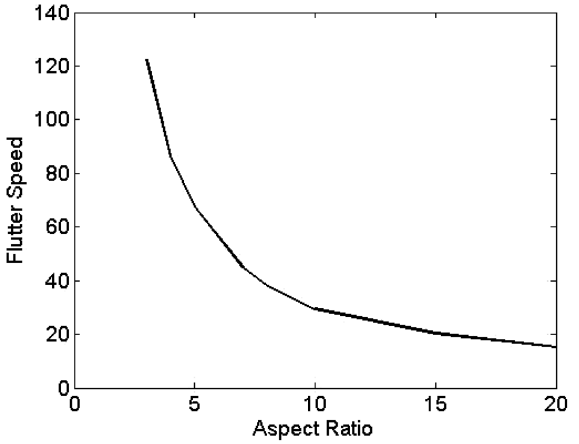

Fig. 9 Flutter speed under a steady freestream as a function of the aspect ratio.

modes (the first bending mode q_1, first torsion mode q_2, second bending mode q_3, and second torsion mode q_4) have been used. Shown in Table 2 are the structural parameters of the plate model used in the current study. These values for the plate model are based on Dunn and Dugundji's work [13]. For the current plate model, the structural natural frequencies are 16.6 (first bending), 60.7 (first torsion), 104.3 (second bending), and 215.3 (second torsion) Hz, respectively. Consequently, to satisfy the Nyquist criteria and capture all of the structural responses in the current system, the sampling frequency must be higher than $2 \times 215.3 = 430.6$ Hz, or Δt should be smaller than $1/430.6 = 0.0023$ s. In the current study, the maximum value of Δt has been set to 0.00059 s.

The mean freestream velocity U_∞ at which the aeroelastic system becomes unstable is called the time-averaged flutter speed. For a plate with an aspect ratio of 4, the magnitude of stream pulsations $\bar{u}$ has been assumed to be zero to calculate the flutter speed under a steady freestream. Kim [9] analyzed a similar plate using a steady vortex lattice model and predicted a flutter speed of 86.3 m/s. The new unsteady vortex lattice model predicts a flutter speed at 85.7 m/s. The two results match well, and the small difference could be due to different structural modes between the two models.

Figure 9 shows the predicted flutter speed under a steady freestream plotted versus the wing's aspect ratio. Increasing the aspect ratio decreases the flutter speed because the increased aspect ratio increases the unsteady aerodynamic forces (Fig. 3) and decreases the wing's structural stiffness. Thus, aeroelastic problems become more important when the aspect ratio is large. Asymptotically, the predicted flutter speed approaches the two-dimensional value as the aspect ratio goes to infinity.

The stability of the aeroelastic system changes as the magnitude and frequency of stream pulsation are varied, and Fig. 10 shows the aeroelastic stability boundaries for mean freestream velocities U_∞ of 70, 75, and 80 m/s when $AR = 4$. These boundaries have been obtained via Floquet analysis of the time-periodic aeroelastic equation [Eq. (25)]. The regions above the boundary lines are unstable, whereas the regions below are stable. For each mean freestream speed, the boundary has peaks and valleys. The valleys represent instabilities resembling the parametric and combinatory resonances, which can occur even at low pulsation magnitudes and

Table 2 Structural parameters of a plate model [13]

Parameters	Values
Chord length	0.0762 m
Span length	0.3048 m
Aspect ratio	4
Material density for plate	3.046 kg/m^2
Thickness of plate	0.002 m
Spanwise bending stiffness	43.33 kg $\cdot$ m^2/s^2
Torsional stiffness	3.756 kg $\cdot$ m^2/s^2

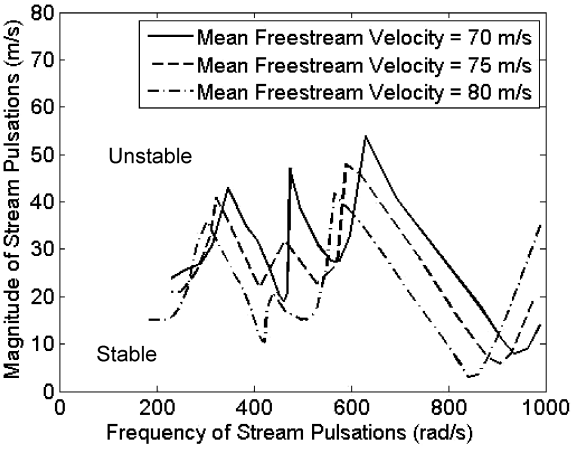

Fig. 10 Flutter boundaries for mean freestream velocities of 70, 75, and 80 m/s.

can lead to potentially dangerous situations [7]. Furthermore, the results suggest that, even at mean freestream velocities below the steady freestream flutter speed of 85.7 m/s, instabilities can occur. The locations of valleys change with mean freestream velocity because system characteristics, including eigenvalues, change. However, the shapes of the flutter boundary curves remain similar. Figure 11 shows the time-averaged flutter speed plotted versus the magnitude of stream pulsations when the frequency of stream pulsations is 800 rad/s. The time-averaged flutter speed decreases

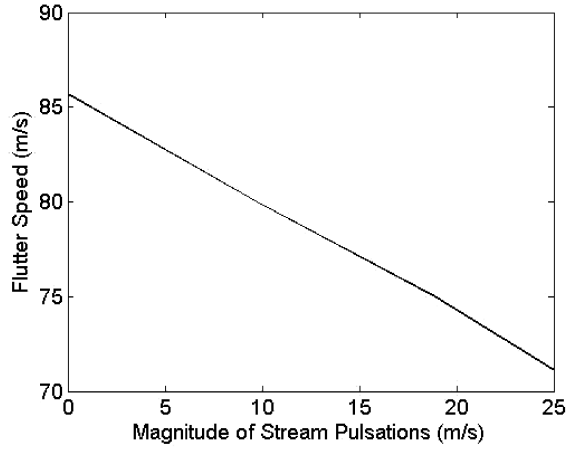

Fig. 11 Flutter speed as a function of the magnitude of stream pulsations when the frequency of stream pulsations is 800 rad/s.

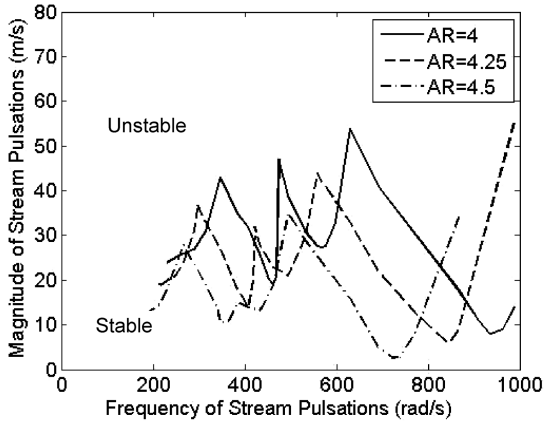

Fig. 12 Flutter boundaries for aspect ratios of 4, 4.25, and 4.5.

linearly as the magnitude of stream pulsations is increased. Thus, increasing the magnitude of stream pulsations destabilizes the aeromechanical system at this pulsation frequency. However, as shown in Fig. 10, the relationship can change when the frequency of stream pulsations is changed.

Also, the stability of the aeroelastic system, including the structural system, changes as the aspect ratio is varied, and Fig. 12 shows the flutter boundary of stream pulsations for three different aspect ratios when $U_\infty = 70$ m/s. For each aspect ratio, three valleys exist. The valleys represent instabilities as in Fig. 10. The locations of valleys change for different aspect ratios because structural characteristics including natural frequencies change as functions of the aspect ratio. In a pulsating freestream, increasing the aspect ratio decreases the stable region because of the same reason as for the steady freestream case (Fig. 9). This type of information can help designers during the early stage of wing design.

C. Forced Response of a Rotating Wing Under a Pulsating Freestream

In this section, an isolated finite wing on a rigid disk which is rotating at a constant speed V is considered (Fig. 13). The time-varying pulsation in the absolute incoming velocity, coupled with a constant rotational speed, results in a time-varying angle of attack as well as a time-varying relative velocity magnitude. Figure 14 shows the transient lift when the steady freestream is suddenly changed into a pulsating freestream with a nondimensional velocity fluctuation

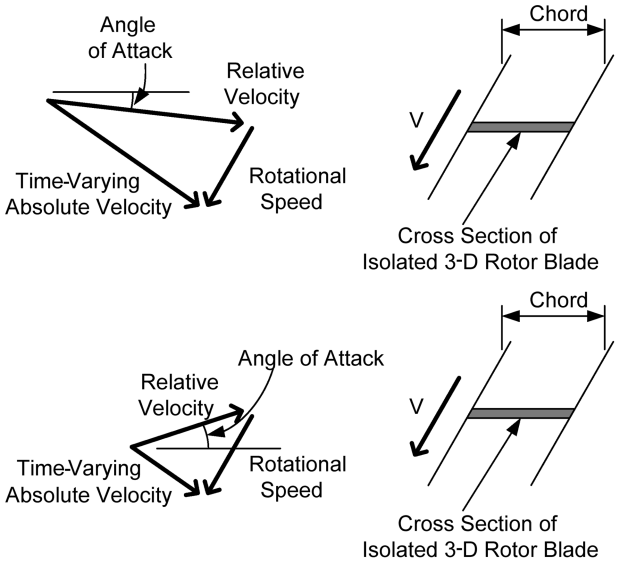

Fig. 13 Velocity triangle for an isolated rotating 3-D wing with a constant rotational speed and time-varying absolute velocity (upper: high absolute velocity case; lower: low absolute velocity case).

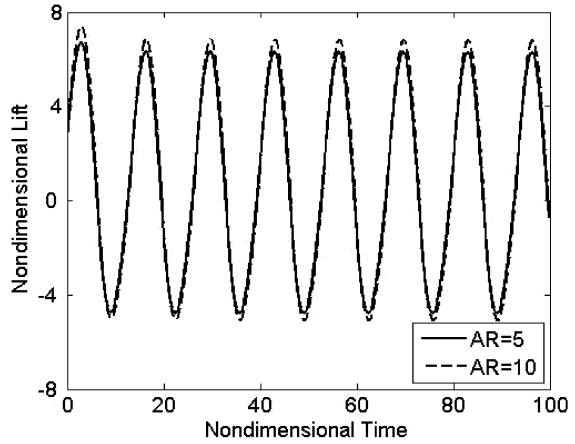

Fig. 14 Transient lift on a rotating wing under a pulsating freestream for aspect ratios of 5 and 10 when $\bar{u}/U_\infty = 0.4$.

amplitude and frequency of 0.4 and 800 rad/s, respectively, at $\tau = 0$. The design flow coefficient has been set to 0.5 and $\bar{u}/U_\infty = 0.4$. The steady-state ($\tau > 20$) and transient ($\tau < 20$) lift both become sinusoidal due to the pulsating angle of attack and pulsating relative velocity magnitude. Like the stationary finite wing in the previous section, the lift pulsation for $AR = 5$ is smaller than that for $AR = 10$.

Figures 15 and 16 show the transient plunge and pitch responses, respectively, when the steady freestream is suddenly changed into a pulsating freestream with $\bar{u}/U_\infty = 0.4$ at $\tau = 0$. These responses are

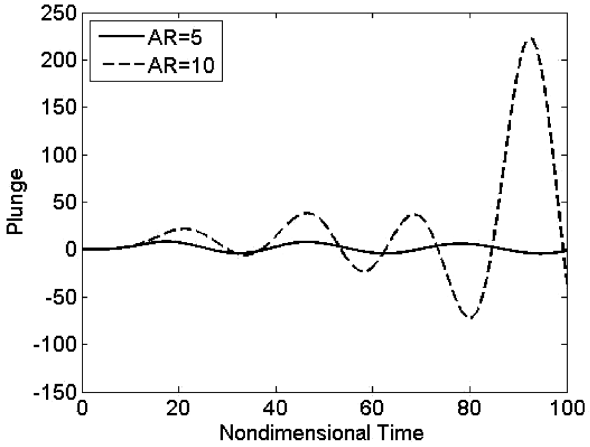

Fig. 15 Transient plunge response of a rotating wing under a pulsating freestream for aspect ratios of 5 and 10 when $\bar{u}/U_\infty = 0.4$.

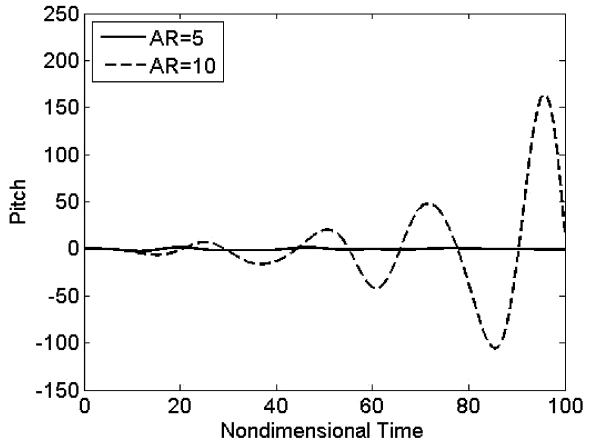

Fig. 16 Transient pitch response of a rotating wing under a pulsating freestream for aspect ratios of 5 and 10 when $\bar{u}/U_\infty = 0.4$.

obtained with aspect ratios of 5 and 10 with an upstream relative velocity of 70 m/s. Again, the flow coefficient U_∞/V has been assumed to be 0.5. For $AR = 5$, a forced vibration exists, but its amplitude does not increase with time. However, the vibration amplitude diverges for $AR = 10$. The critical aspect ratio at which the vibration amplitude begins to diverge has been calculated to be 6.8. Thus, the increasing aspect ratio of a rotating finite wing adversely affects the wing's forced response as well.

IV. Conclusions

A new three-dimensional unsteady vortex lattice model has been developed to analyze the unsteady aerodynamic forces and aeroelastic stability of an isolated three-dimensional wing under pulsating freestream conditions. The conclusions of this paper can be summarized as follows:

1) The nondimensional lift under both steady and pulsating freestream increases as the aspect ratio is increased.
2) In a steady freestream, the flutter speed is inversely proportional to the aspect ratio.
3) In a pulsating freestream, the increasing magnitude of stream pulsations destabilizes the aeroelastic system.
4) At certain resonant frequencies, even a small stream pulsation can trigger aeroelastic instability.
5) With a pulsating freestream, flutter can occur at mean freestream speeds below the flutter speed of the steady freestream case.
6) In a pulsating freestream, increasing the aspect ratio decreases the stable region.
7) For a rotating finite wing, the time-varying angle of attack causes a forced response as well as flutter, and forced response is also worsened as the aspect ratio increases.

Acknowledgments

The authors are grateful to Sang Joon Shin of Seoul National University for his helpful comments. Also, the authors gratefully acknowledge financial support from the BK 21 Project, the Microthermal System Research Center of the Korea Science and Engineering Foundation, the Institute of Advanced Machinery and Design of Seoul National University, and the Agency for Defense Development (Contract monitor, Yeong Ryun Kim).

References

[1] Hall, K. C., "Eigenanalysis of Unsteady Flows about Airfoils, Cascades, and Wings," *AIAA Journal*, Vol. 32, No. 12, 1994, pp. 2426–2432.
doi:10.2514/3.12309

[2] Kim, T. H., Nam, C. H., and Kim, Y. D., "Reduced-Order Aeroservoelastic Model with an Unsteady Aerodynamic Eigen Formulation," *AIAA Journal*, Vol. 35, No. 6, 1997, pp. 1087–1088.
doi:10.2514/2.201

[3] Isaacs, R., "Airfoil Theory for Flows of Variable Velocity," *Journal of the Aeronautical Sciences*, Vol. 12, No. 1, 1945, pp. 113–117.

[4] Greenberg, J. M., "Airfoil in Sinusoidal Motion in Pulsating Stream," National Advisory Com. for Aeronautics, TN 1326, 1947.

[5] Theodorsen, T., "General Theory of Aerodynamic Instability and the Mechanism of Flutter," National Advisory Com. for Aeronautics Rept. No. 496, 1935.

[6] Dugundji, J., and Bundas, D. J., "Flutter and Forced Response of Mistuned Rotors Using Standing Wave Analysis," *AIAA Journal*, Vol. 22, No. 11, 1984, pp. 1652–1661.
doi:10.2514/3.8832

[7] Cho, S. H., Kim, T., Song, S. J., and Shin, S. J., "Aeroelastic Analysis of an Isolated Airfoil Under a Pulsating Flow," *AIAA Journal*, Vol. 45, No. 5, 2007, pp. 1000–1006.
doi:10.2514/1.25485

[8] Katz, J., and Plotkin, A., *Low-Speed Aerodynamics*, 2nd ed., Cambridge Univ. Press, Cambridge, England, U.K., 2001.

[9] Kim, T., "Methods of Aeroservoelastic Formulation: Industrial Practices," Short Course given at the *46th AIAA/ASME/ASCE/AHS/ASC Structures, Structural Dynamics and Materials Conference*, April 2005.

[10] Bolotin, V. V., *The Dynamic Stability of Elastic Systems*, Holden–Day, San Francisco, 1964.

[11] Bisplinghoff, R. L., Ashley, H., and Halfman, R. L., *Aeroelasticity*, 1st ed., Dover, New York, 1996.

[12] Anderson, J. D., Jr., Corda, S., and van Wie, D. M., "Numerical Lifting Line Theory Applied to Drooped Leading-Edge Wings Below and Above Stall," *Journal of Aircraft*, Vol. 17, No. 12, 1980, pp. 898–904.
doi:10.2514/3.44690

[13] Dunn, P. E., and Dugundji, J., "Nonlinear Stall Flutter and Divergence Analysis of Cantilevered Graphite/Epoxy Wings," *AIAA Journal*, Vol. 30, No. 1, 1992, pp. 153–162.
doi:10.2514/3.10895

C. Cesnik
Associate Editor